Solar-sail quasi-periodic orbits in the sun–earth system

Mora, Alvaro Fernandez; Heiligers, Jeannette

DOI
10.2514/1.G005021

Publication date
2020

Document Version
Accepted author manuscript

Published in
Journal of Guidance, Control, and Dynamics

Citation (APA)
Mora, A. F., & Heiligers, J. (2020). Solar-sail quasi-periodic orbits in the sun–earth system. *Journal of Guidance, Control, and Dynamics*, *43*(9), 1740-1749. https://doi.org/10.2514/1.G005021

Solar-Sail Quasi-Periodic Orbits in the Sun-Earth System

Alvaro Fernandez Mora * and Jeannette Heiligers †
Delft University of Technology, Delft, 2629 HS, the Netherlands.

Nomenclature

Latin Symbols

J_c	Jacobi constant	-
L_i	Lagrange point for $i \in \{1, 2, ...5\}$	-
M	Monodromy matrix	-
R	Rotation operator	-
s_i	Stability index for $i \in \{1, 2\}$	-
SL_i	Displaced Lagrange points for $i \in \{1, 2, ..., 5\}$	-

Greek Symbols

α	Cone angle	rad
β	Lightness number	-
δ	Clock angle	rad
$\boldsymbol{\theta}$	Vector of angular variables	rad
μ	Gravitational parameter	-
ρ	Rotation number	rad
ϕ_t	Flow for time t	-
Φ	State transition matrix	-
ψ	Parameterization of invariant torus	-
$\boldsymbol{\omega}$	Vector of frequencies	rad
φ	Parameterization of invariant curve	-

*Graduate student, Department of Astrodynamics and Space Missions, Faculty of Aerospace Engineering
†Assistant professor, Department of Astrodynamics and Space Missions, Faculty of Aerospace Engineering

I. Introduction

Bounded motion in the Circular Restricted Three-Body Problem (CR3BP) is of particular interest for the preliminary design of space missions. Periodic orbits around the Lagrange points are well understood, see Ref. [1] for a detailed survey, and such knowledge has been leveraged and combined with mission design techniques for practical applications. Space-weather spacecraft in orbits around the L_1 point like SOHO, ACE, WIND and DSCOVR and astronomic observatories at the Sun-Earth L_2 point like GAIA are clear examples. However, quasi-periodic orbits can be more suitable for space missions than periodic orbits for space missions as they might require less station keeping, extend the mission design space and allow for new transfer opportunities: whereas at fixed energy levels only a finite number of periodic orbits exists, entire families of quasi-periodic orbits exist around each such periodic orbit [2, 3]. Extensive research has been conducted on the conditions for existence of quasi-periodic motion in the CR3BP and their evolution [2, 4]. Furthermore, several methods for the computation of families of quasi-periodic orbits have been developed, including partial differential equations solvers, invariant curves of Poincaré and stroboscopic maps [5, 6] and center manifold reductions [4].

The CR3BP neglects a wide variety of dynamical effects such as solar radiation pressure (SRP); the effect of SRP can become significant for bodies with a large area-to-mass ratio like solar-sail spacecraft. These probes are propelled by the force exerted by SRP on a highly reflective surface [7]. Solar-sail technology has developed rapidly over the past decades resulting in solar-sail spacecraft like IKAROS (JAXA), NanoSail D2 (NASA) and LightSail 1 and 2 (The Planetary Society) and the upcoming NEA Scout (NASA) mission.

For the CR3BP+SRP case, only few studies have explored quasi-periodic orbits by means of a center manifold reduction combined with Poincaré sections exclusively for a particular lightness number in the vicinity of the displaced L_1 point [8, 9]. We build on these initial investigations and extend the results in Refs. [8, 9] to analyzing the conditions for existence of solar-sail quasi-periodic orbits in the vicinity of the displaced L_1, L_2 and L_5 points, all for the case where the sail is oriented perpendicular to the direction of sunlight. We compute entire families of solar-sail quasi-periodic orbits around these displaced Lagrange points and present the first-ever extensive investigation of solar-sail periodic and quasi-periodic orbits with the solar-sail lightness number. To this end, we extend the application of the method of invariant curves under stroboscopic maps, developed in Refs. [2, 10] for the CR3BP, to the CR3BP+SRP dynamical framework. The motivation for choosing the method of invariant curves under stroboscopic maps lies in the fact that the results from this method can be directly used for mission design purposes. Indeed, the results from the method of stroboscopic maps are conceptually very different from those obtained with the centre manifold reduction technique in Refs. [8, 9]. In particular, in Refs. [8, 9], the center manifold is sampled at Poincaré sections and as a result only points in periodic and quasi-periodic orbits are obtained in center manifold coordinates. Instead, through the stroboscopic mapping method, invariant curves (in Fourier expansions) are obtained, each defining an invariant torus, allowing the quasi-periodic orbits to be obtained explicitly instead of implicitly as in the centre manifold reduction technique. The

results obtained in this Note therefore offer a catalog on solar-sail quasi-periodic orbits that can be directly used for mission design to set quasi-periodic orbits as departure or arrival invariant objects [3].

II. Dynamical System

In order to model the motion of the solar-sail propelled spacecraft (hereafter referred to as "solar sail"), we consider the dynamical framework of the CR3BP perturbed with an acceleration induced by solar radiation pressure. In such a model, the Sun and the Earth (primary bodies) move in circular orbits around their common barycenter, exclusively attracting each other. The motion of the solar sail (third body) is governed by the vector field induced by the gravitational pull of the primaries and the SRP. The primaries are assumed to be point masses and the solar sail is assumed to be massless. The units of mass, distance and time are normalized such that the total mass of the system is 1, the Sun-Earth distance is 1 and the orbital period of the Earth around the Sun is 2π. With these normalized units, the gravitational parameter of Earth becomes $\mu = 3.0034806 \cdot 10^{-6}$ and the gravitational parameter of the Sun becomes $1 - \mu$.

We consider a synodic reference frame $S(\hat{\boldsymbol{x}}, \hat{\boldsymbol{y}}, \hat{\boldsymbol{z}})$ with basis $\{\hat{\boldsymbol{x}}, \hat{\boldsymbol{y}}, \hat{\boldsymbol{z}}\}$ to study the system. The origin is at the Sun-Earth barycenter, the $x-$axis, and $\hat{\boldsymbol{x}}$, are defined along the Sun-Earth line pointing towards the Earth, the $z-$axis, and $\hat{\boldsymbol{z}}$, are defined in the direction of the angular momentum vector of the primaries and the $y-$axis, and $\hat{\boldsymbol{y}}$, complete the orthogonal right-handed reference frame, see Fig. 1a. In this frame, the equations of motion can be obtained as:

$$\ddot{x} - 2\dot{y} = \frac{\partial \Omega}{\partial x} + a_x, \tag{1}$$

$$\ddot{y} + 2\dot{x} = \frac{\partial \Omega}{\partial y} + a_y, \tag{2}$$

$$\ddot{z} = \frac{\partial \Omega}{\partial z} + a_z, \tag{3}$$

with $\Omega = \frac{1}{2}\left(x^2 + y^2\right) + \frac{1-\mu}{r_{sb}} + \frac{\mu}{r_{eb}}$, $r_{sb} = \sqrt{(x+\mu)^2 + y^2 + z^2}$ and $r_{eb} = \sqrt{(x+\mu-1)^2 + y^2 + z^2}$. Note that r_{sb} and r_{eb} are the norms of the Sun-body vector, $\boldsymbol{r}_{sb} = [x+\mu \quad y \quad z]^T$, and of the Earth-body vector, $\boldsymbol{r}_{eb} = [x+\mu-1 \quad y \quad z]^T$, respectively. The acceleration generated by the solar sail is defined as the vector $\boldsymbol{a} = [a_x \quad a_y \quad a_z]^T$. We assume a perfectly reflecting flat "ideal" sail and a uniformly radiating Sun. For an ideal sail, the solar-sail acceleration acts along the direction of the sail normal and is conveniently expressed as a function of the lightness number β. This parameter is defined as the ratio between the solar-sail and solar-gravitational accelerations [7]. Near-term values for this lightness number are $\beta \leq 0.04$ [11]. Note that more complex solar-sail models exist [7, 12] but that for the initial analyses in this work, the ideal model is deemed sufficient. The solar-sail acceleration can then be described in dimensionless units as:

$$\boldsymbol{a} = \beta \frac{1-\mu}{r_{sb}^2} \langle \hat{\boldsymbol{r}}_{sb}, \hat{\boldsymbol{n}} \rangle^2 \hat{\boldsymbol{n}}, \tag{4}$$

where $\hat{\boldsymbol{r}}_{sb} = \frac{\boldsymbol{r}_{sb}}{r_{sb}}$ and $\hat{\boldsymbol{n}}$ is the sail normal unit vector, see Fig. 1a.

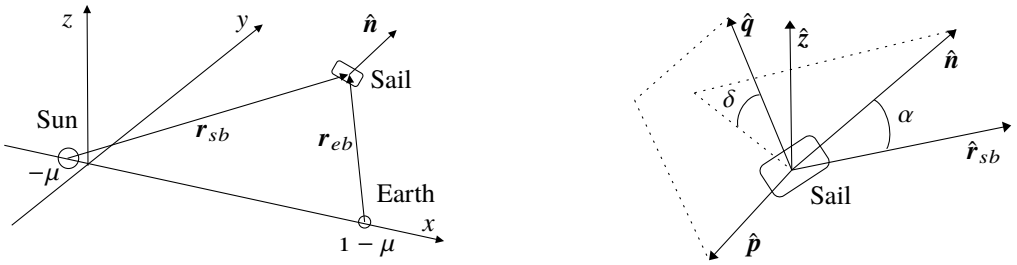

Fig. 1 a) Sketch of the synodic reference frame and b) sketch of the local frame used to define the cone angle α and the clock angle δ.

In order to describe the sail normal $\hat{\boldsymbol{n}}$ in the synodic frame, we follow Ref. [13] and define a reference frame $s(\hat{\boldsymbol{r}}_{sb}, \hat{\boldsymbol{p}}, \hat{\boldsymbol{q}})$ with its origin at the solar sail and basis $\{\hat{\boldsymbol{r}}_{sb}, \hat{\boldsymbol{p}}, \hat{\boldsymbol{q}}\}$, where $\hat{\boldsymbol{p}} = \frac{\hat{\boldsymbol{r}}_{sb} \times \hat{\boldsymbol{z}}}{|\hat{\boldsymbol{r}}_{sb} \times \hat{\boldsymbol{z}}|}$ and $\hat{\boldsymbol{q}} = \frac{\hat{\boldsymbol{p}} \times \hat{\boldsymbol{r}}_{sb}}{|\hat{\boldsymbol{p}} \times \hat{\boldsymbol{r}}_{sb}|}$. The sail normal can then be described in this frame by two angles, known in the literature as the cone angle α and the clock angle δ. Note that, since the solar sail is unable to generate an acceleration towards the Sun, $\alpha \in [-\pi/2, \pi/2]$ and $\delta \in [0, \pi]$. Figure 1b shows the reference frame centered at the solar sail as well as the cone and clock angles.

While the CR3BP is Hamiltonian, the solar-sail perturbation breaks this property of the system, although a few exceptions exist: when the sail normal is aligned with the direction of the Sun-sail line ($\alpha = 0$) and when the sail normal is perpendicular to the Sun-sail line ($\alpha = \pm\pi/2$). Note that the latter case will result in a zero solar-sail acceleration and can thus be represented by a lightness number $\beta = 0$. For these cases, the existence of periodic and quasi-periodic motion around the equilibrium points is guaranteed [13]. Another important aspect of the dynamical system when the Hamiltonian structure is preserved is the existence of a first integral known as the Jacobi constant [13]. This constant of motion has important implications for the characterization of regions of possible motion and energy levels of periodic and quasi-periodic orbits, where the effect of the latter will be discussed in Section IV.

We can now express Eqs. 1-3 as a system of first order differential equations given by $\dot{\boldsymbol{x}} = f(\boldsymbol{x}, \alpha, \delta)$, with $\boldsymbol{x} \in \mathbb{R}^6$. We can also define the flow induced by f as $\phi_t(\boldsymbol{x}, \alpha, \delta)$ with $t \in \mathbb{R}$. Note that in this system, several equilibrium points exist, i.e., $f(\boldsymbol{x}, \alpha, \delta) = 0$. When $\alpha = \pm\pi/2$ (or $\beta = 0$), the well known Lagrange points satisfy such a condition. When $\alpha = 0$, the Lagrange points are displaced and are known as displaced Lagrange points denoted by SL_i with $i \in \{1, 2, ..., 5\}$, which highly resemble their classical counterparts [8].

III. Periodic Orbits

For the computation of quasi-periodic orbits, an understanding of periodic motion is necessary. This section aims to introduce those notions on periodic orbits that will later be used for the computation of quasi-periodic orbits.

Periodic orbits generally appear in continuous families. Numerous studies have used symmetric properties of the system to compute families of periodic orbits in the classical system, e.g., [14, 15], and in the SRP-perturbed system,

e.g., [16, 17]. We, however, do not exploit orbit symmetry. Instead, a very general way to impose periodic motion is given by the definition of the map $G : \mathbb{R}^7 \rightarrow \mathbb{R}^6$ as [18]

$$G(\boldsymbol{x}, T) = \phi_T(\boldsymbol{x}, \alpha, \delta) - \boldsymbol{x}. \tag{5}$$

Note that, in this work, the sail attitude is constant for each family of periodic orbits and therefore α and δ are fixed parameters of the map G. More specifically, two particular sail attitudes are considered: $\alpha = 0$ and $\alpha = \pm\pi/2$. For both these attitudes, the clock angle, δ, has no effect on the dynamics and it is therefore not defined. Furthermore, the case $\alpha = 0$ allows for passive solar-sail attitude control through a correct offset between the center of pressure and center of mass [7]. Finally, the case $\alpha = \pm\pi/2$ does not generate any solar-sail acceleration and will therefore be represented in this work through a lightness number equal to $\beta = 0$.

The search for periodic orbits is then transformed into finding $\{\boldsymbol{x}, T\}$ that solve $G(\boldsymbol{x}, T) = \boldsymbol{0}$. Then, $\boldsymbol{x}$ belongs to a periodic orbit with period T given that $T > 0$. Such solutions can be found with a Newton method from a good initial guess. Furthermore, once a solution is found, the families of periodic orbits can be continued. For more details on the initial guess, the Newton method and the continuation, see Ref. [3].

A. Orbit stability

An important feature of periodic orbits is their stability, which can be assessed from the eigenvalues of the monodromy matrix. Such a matrix can be seen as a linear map between the variation of the initial conditions of a flow and the variation on the final conditions. Because of the properties of the monodromy matrix, the spectra for solar-sail Hamiltonian periodic orbits have the form $spec(M) = \{1, 1, \lambda_1, \lambda_1^{-1}, \lambda_2, \lambda_2^{-1}\}$ [8]. The stability indices are then defined as $s_i = |\lambda_i + \lambda_i^{-1}|$. With such a definition, a periodic orbit can be described as [8]:

1) Hyperbolic: $s_i > 2$.
2) Elliptic: $s_i \leq 2$. When $s_i = 2$, periodic orbits are said to have a central part.
3) Complex unstable: if $\lambda_i \in \mathbb{C}\backslash\mathbb{R}$ and $|\lambda_i| \neq 1$.

A periodic orbit is said to be stable if $s_i \leq 2$ for $i \in \{1, 2\}$. Elliptic periodic orbits with a central part are important for the study on the existence of families of quasi-periodic orbits since around such periodic orbits quasi-periodic motion exists [8].

B. Periodic orbit families

Although many periodic orbit families exist [1], we only consider the planar Lyapunov, vertical Lyapunov and halo families for demonstration purposes with special emphasis on the evolution of their stability to identify orbits with a central part. We compare the stability indices in logarithmic scale against a normalized Jacobi constant, j_c. The

normalized Jacobi constant is defined as J_c divided by the maximum absolute value of J_c encountered in the family. The use of j_c is convenient for comparing the stability indices of families for different lightness number as all curves can be represented together in a clear way, see Fig. 3 for example. Generally, for the families considered in this Note, the Jacobi constant (and also j_c) increases throughout the continuation; therefore, the smallest value of j_c is found for the orbits closest to the equilibrium point, i.e., at the start of the families, and as the families are continued, the (normalized) Jacobi constant increases. This general rule applies for the planar and vertical Lyapunov families around the SL_1 and SL_2 points and for the halo families around the SL_1 point.

1. Planar Lyapunov families around SL_1 and SL_2

In order to illustrate the planar Lyapunov families, Fig. 2 shows subsets of the families around the SL_1 point (Fig. 2a) and the SL_2 point (Fig. 2b) for $\beta = 0.04$. The orbits are plotted in a color-scale based on their value of j_c. It can be seen how both families begin at $j_c = -1$, close to the corresponding equilibrium point, and that the normalized Jacobi constant increases throughout the continuation while the orbits grow in size. Regarding the stability of the planar

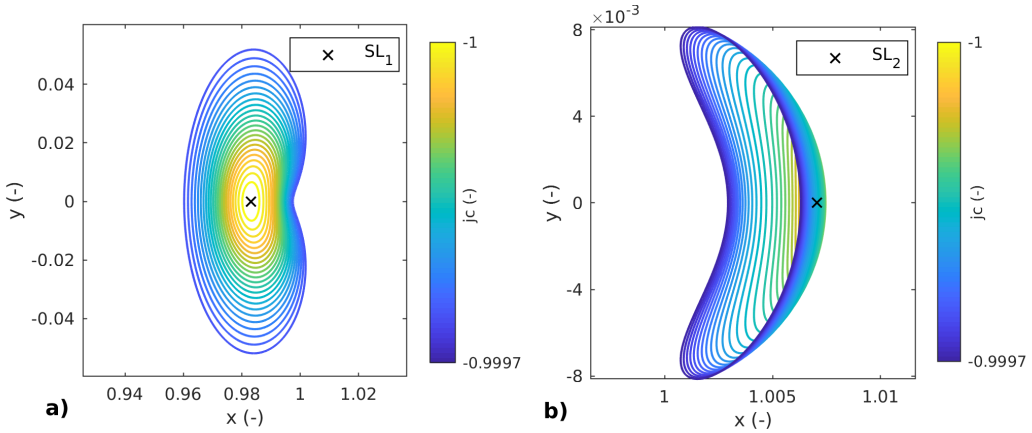

Fig. 2 Planar Lyapunov families for $\beta = 0.04$: a) around SL_1 and b) around SL_2.

Lyapunov families, Fig. 3 shows both stability indices, as a function of j_c for several values of β. The figure shows that $s_1 > 2$ for all orbits around both the SL_1 and SL_2 points and they are therefore unstable. Additionally, the orbits at the smallest values of j_c have a central part, i.e., $s_2 = 2$. When the orbits increase in j_c, this characteristic is lost but it is subsequently regained for larger values of j_c.

2. Vertical Lyapunov families around SL_1 and SL_2

In Fig. 4, the vertical Lyapunov families around the SL_1 point (Fig. 4a) and the SL_2 point (Fig. 4b) are shown for $\beta = 0.04$. Some orbits that present an extra loop with respect to the traditional eight-shaped vertical Lyapunov orbits appear midway of the family, but such extra loop is subsequently lost. One such orbit is depicted in black in Fig. 4a. Note that this double-loop behavior is not specific to the solar-sail case as we found similar behavior for $\beta = 0$, i.e., the

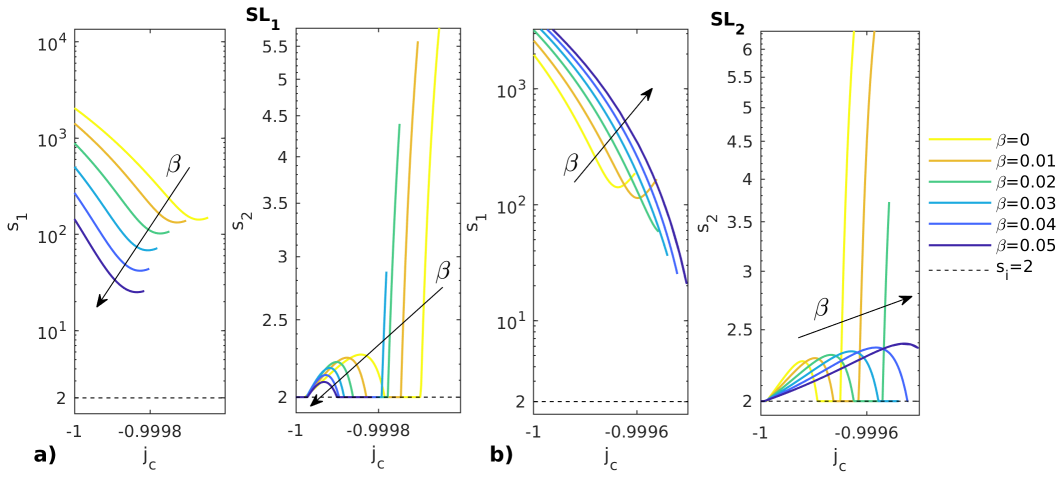

Fig. 3 Stability indices for the planar Lyapunov families in logarithmic scale for $\beta \in \{0, 0.01, ..., 0.05\}$ with the arrow in the direction of increasing β: a) around SL_1 and b) around SL_2.

CR3BP case.

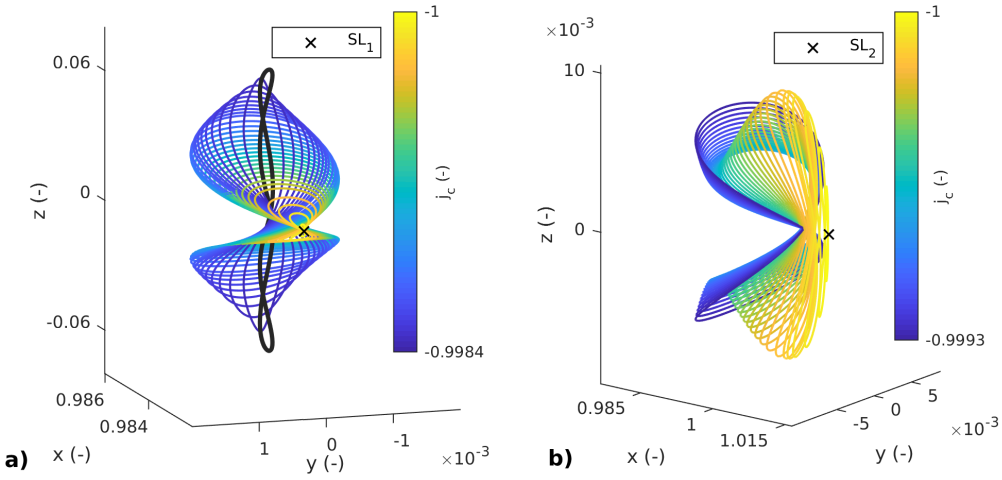

Fig. 4 Vertical Lyapunov families for $\beta = 0.04$: a) around SL_1 and b) around SL_2.

The stability indices for the vertical Lyapunov families are shown in Fig. 5, where it can be seen that the families around both the SL_1 and SL_2 points are again unstable since no orbit exists with both $s_1 \leq 2$ and $s_2 \leq 2$. Note that for the family around SL_2 and $\beta = 0.05$, when $s_1 = 2$, $s_2 \neq 2$. In fact, we found that this particular case corresponds to the bifurcation point where the vertical Lyapunov orbits become planar. Such a bifurcation does not exist in the CR3BP or for $\beta \leq 0.04$. Also note that the orbits again have a central part at the start of the families, where $j_c \approx -1$, that is eventually lost when the Jacobi constant increases.

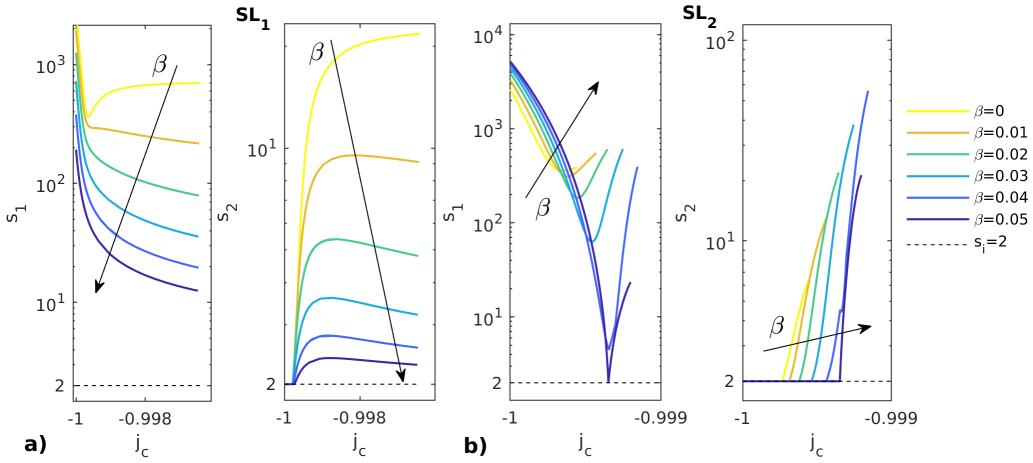

Fig. 5 Stability indices for the vertical Lyapunov families in logarithmic scale for $\beta \in \{0, 0.01, ..., 0.05\}$ with the arrow in the direction of increasing β: a) around SL_1 and b) around SL_2.

3. Halo families around SL_1 and SL_2

Without loss of generality, we focus on the northern branch of the halo families. As an example, Fig. 6 shows the northern halo families around the SL_1 point (Fig. 6a) and the SL_2 point (Fig. 6b) for $\beta = 0.04$. A change in the shape with respect to the classical (i.e., $\beta = 0$) halo family around the L_1 point can be seen as the family collapses onto the ecliptic plane instead of finishing as near-rectilinear halo orbits as is the case for the classical family [14]. In fact, there are several branches in the halo family around SL_1; some of which bifurcate into planar families [19]. It is interesting to note that the northern halo families around SL_2 are the only families in this Note where the smallest value of the Jacobi constant is reached for the orbit at the end of the family (for $\beta > 0$), see Fig 6b for $\beta = 0.04$. Therefore, the families for such lightness numbers end at $j_c = -1$. Instead, for $\beta = 0$, the smallest Jacobi constant is reached at the start of the family; thus, the family starts at $j_c = -1$. The stability indices for the northern halo families around the SL_1 and the SL_2 points are shown in Fig. 7. Note the different behavior for the stability index s_1 for the family around SL_2 and $\beta = 0$, see Fig. 7b. It can also be seen that there are stable northern halo orbits around both SL_1 and SL_2 as there are orbits with $s_1 = 2$ and $s_2 = 2$. Also note that for the families around SL_1 and $\beta \in \{0, 0.04, 0.05\}$, s_2 stays on the line $s_2 = 2$ or very close to it whereas this is not the case for the remaining lightness numbers. For the families around SL_2, the stable halo orbits emerge when the families approach near rectilinear halo orbits at the end of the families. Finally, note that the orbits in the families around SL_2 always have a central part as $s_2 = 2$ for all β. Figure 7 also shows that for some lightness numbers the stability indices intersect with the line $s_i = 2$ more than once, suggesting an interesting behavior which might be accounted for by the bifurcations existing in the halo family [19].

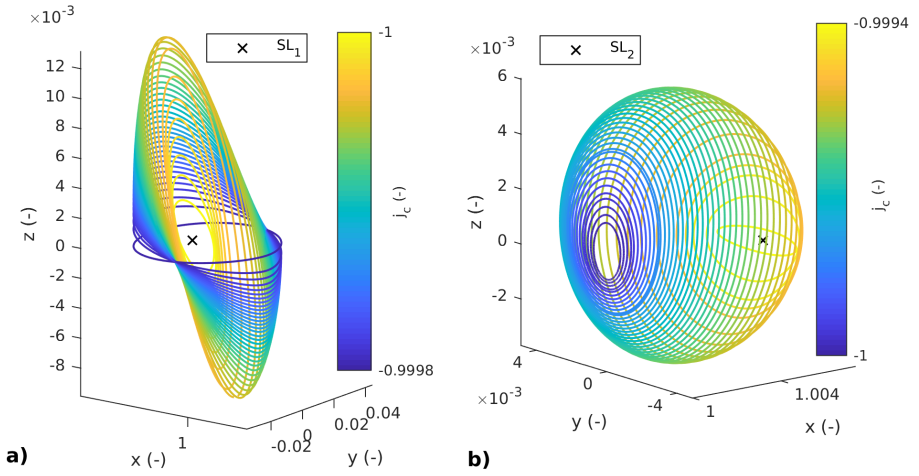

Fig. 6 Northern halo families for $\beta = 0.04$: a) around SL_1 and b) around SL_2.

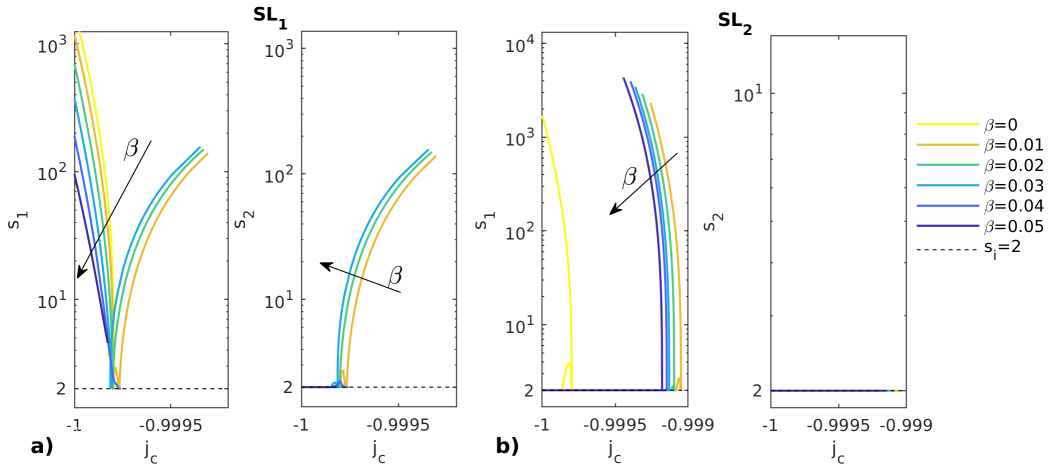

Fig. 7 Stability indices for the northern halo families in logarithmic scale for $\beta \in \{0, 0.01, ..., 0.05\}$ with the arrow in the direction of increasing β: a) around SL_1 and b) around SL_2.

4. Lyapunov families around SL_5

Lastly, two orbit families originate from the SL_4 and SL_5 points: the planar and vertical Lyapunov families. Figure 8 shows the planar family (Fig. 8a) and the vertical one (Fig. 8b) around the SL_5 point for $\beta = 0.04$. A plot of the stability indices is omitted because these families are stable for all β since the orbits are always elliptic, i.e., $s_1 = 2$ and $s_2 = 2$.

IV. Invariant Tori

The Arnold-Liouville theorem proves that under certain conditions, trajectories of a dynamical system lie on an invariant manifold on the phase space which is diffeomorphic to the n-dimensional torus [20]. A corollary of the Arnold-Liouville theorem is that for an integrable system, bounded trajectories are contained on a torus where both periodic and quasi-periodic orbits may exist. Neither the CR3BP nor the CR3BP+SRP are integrable, so the

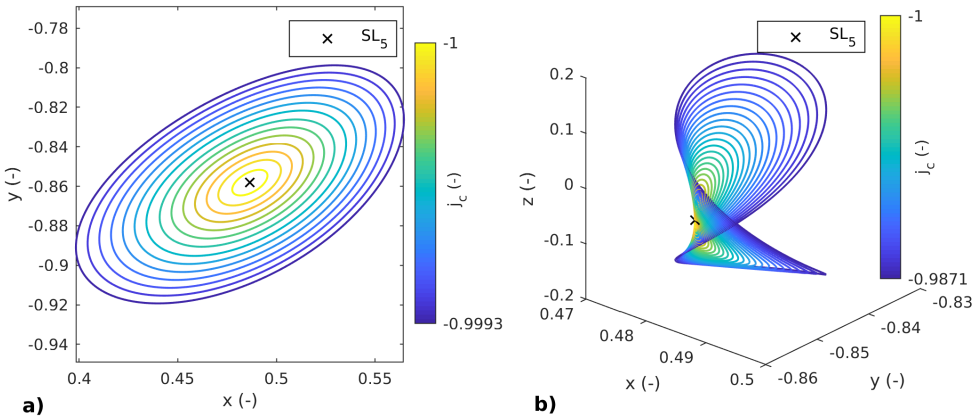

Fig. 8 Lyapunov families around SL_5 for $\beta = 0.04$: a) planar and b) vertical orbits.

Arnold-Liouville theorem does not apply. It is not unreasonable to think that quasi-periodic orbits could still exist in perturbations of integrable systems. In fact, KAM theory shows that, under certain conditions, this is indeed the case [4]. Therefore, we explore 2-dimensional tori for the solar-sail attitude cases outlined in Section III: $\alpha = 0$ and $\alpha = \pm\pi/2$, i.e., $\beta = 0$. For the non-Hamiltonian case, Refs. [8, 9] have demonstrated that quasi-periodic orbtis also exist for sail attitudes close to $\alpha = 0$ where the system is time-reversible. We are interested in a parameterization $\psi : \mathbb{T}^2 \rightarrow \mathbb{R}^6$ such that [2]

$$\psi(\boldsymbol{\theta} + \boldsymbol{\omega} t) = \phi_t(\psi(\boldsymbol{\theta}), \alpha, \delta), \tag{6}$$

where $\boldsymbol{\theta} = [\theta_1 \quad \theta_2]^T \in \mathbb{R}^2$ parameterizes the torus and $\boldsymbol{\omega} = [\omega_1 \quad \omega_2]^T \in \mathbb{R}^2$ is the vector of frequencies. Figure 9 depicts the torus domain together with a possible choice for θ_1 and θ_2 that is mapped to the quasi-periodic orbits under ψ. Instead of looking for a parameterization of the full torus, it is possible to reduce the dimension of the problem

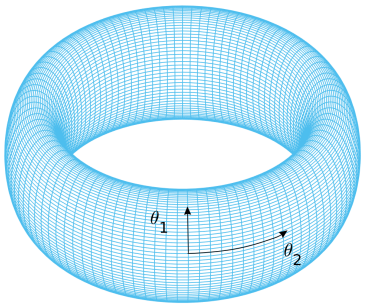

Fig. 9 Representation of a torus domain and a choice for θ_1 and θ_2.

by looking for a parameterization of an invariant curve $\varphi : \mathbb{T}^1 \rightarrow \mathbb{R}^6$ under the stroboscopic map ϕ_{T_2}, where T_2 is the period associated with the frequency ω_2. The invariance condition for the curve under ϕ_{T_2} can be expressed as

$$\varphi(\xi + \rho) = \phi_{T_2}(\varphi(\xi), \alpha, \delta), \tag{7}$$

where ρ is the rotation number and ξ is the parameter that parameterizes φ. Note that the rotation number and T_2 are related as $\rho = \omega_1 T_2$ [2].

A parameterization of an invariant curve can be obtained with a complex truncated Fourier series as

$$\varphi(\xi) = \sum_{k \in K} \boldsymbol{c}_k e^{ik\xi}, \tag{8}$$

where K is an index set and $\boldsymbol{c}_k$ are the complex Fourier coefficients [10]. By discretizing ξ into N values ξ_j with $j \in \{1, 2, ..., N\}$, it is possible to discretize the invariant curve into N points $\varphi(\xi_j)$. Consequently, by means of the discrete Fourier transform (DFT), there is a linear transformation between the complex coefficients $\boldsymbol{c}_k$ of the Fourier series and the discretized invariant curve. Expressing the coefficients and the discretized curve as the column vectors $\boldsymbol{c}$ and $\bar{\boldsymbol{\varphi}}$, respectively, yields the relation $\boldsymbol{c} = D\bar{\boldsymbol{\varphi}}$, where D is the linear operator for the DFT [10]. In this Note we use $N = 35$; therefore, the invariant curves are discretized into 35 points and expressed in a Fourier series up to degree 35. In order to meet the invariance condition expressed in Eq. 7, a rotation operator R is used to rotate the mapped curve under the stroboscopic map over an angle $-\rho$, i.e.,

$$R(-\rho) \circ \phi_{T_2}(\varphi(\xi), \alpha, \delta) - \varphi(\xi) = \mathbf{0}. \tag{9}$$

The rotation can be performed by first obtaining the Fourier coefficients of the mapped discretized curve, then transforming each coefficient with another operator $Q(-\rho) : \boldsymbol{c}_k \rightarrow \boldsymbol{c}_k e^{-ik\rho}$ and finally obtaining the states in the rotated curve. Consequently, $R(-\rho) = D^{-1}Q(-\rho)D$ [10].

To ensure that the invariant curve defines a quasi-periodic orbit, it is necessary that all points of the curve have the same Jacobi constant. Therefore, each point of the invariant curve is constrained to $J_c(\varphi(\xi_j)) = J_c^{fixed}$. Given a good initial guess, the invariance condition from Eq. 9 together with the Jacobi constraint can be used in a Newton method to obtain invariant curves together with the rotation number ρ and the period T_2. Figure 10 shows a discretized guess $\bar{\varphi}(\xi)$ for an invariant curve and its image under the stroboscopic map (Fig. 10a) and the converged solution and its image (Fig. 10b) for a tolerance on Eq. 9 of 10^{-10} after three iterations of the Newton method. From the converged solution, it can be appreciated how the flow comes back to the same curve.

In order to apply the method described, an initial guess is required. Let us assume a periodic orbit defined by a phase space point $\boldsymbol{x}_p$ and a period T. If such an orbit has a central part, then the eigenplane passing through $\boldsymbol{x}_p$ associated with the eigenvalues λ_i and λ_i^{-1} contains invariant curves of the linearization around $\boldsymbol{x}_p$ of a stroboscopic map with stroboscopic time $T_2 = T$, i.e., the monodromy matrix. Some of these invariant curves subsist in the full system, giving rise to invariant tori around periodic orbits [2]. Therefore, given λ_i an eigenvalue within the unit circle,

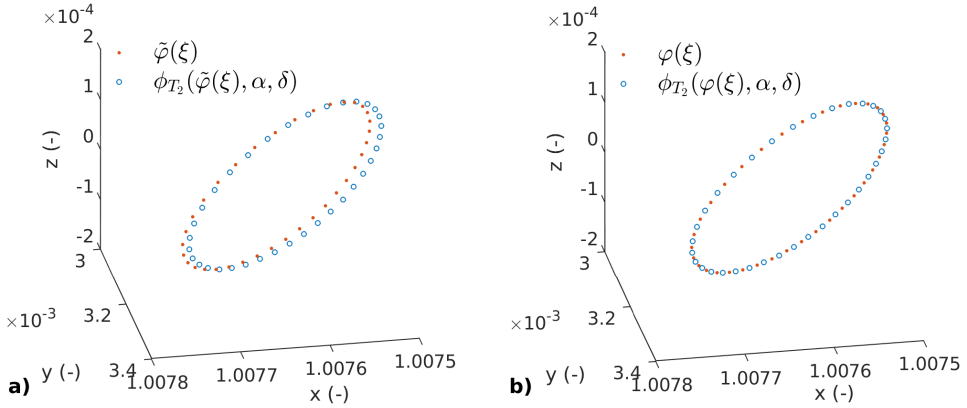

Fig. 10 a) Guess for an invariant curve and its image under the stroboscopic map and b) the converged solution and its image.

and the associated complex eigenvector $\boldsymbol{y}$, the initial guess can be obtained as [10]

$$\tilde{\varphi}(\xi) = \boldsymbol{x}_p + \rho_\epsilon [\cos(\xi) Re(\boldsymbol{y}) - \sin(\xi) Im(\boldsymbol{y})], \tag{10}$$

where ρ_ϵ is the radius of the initial guess for the invariant curve, which is taken as 10^{-7} in dimensionless units. For the rotation number, it can be shown that the phase of λ_i can be used as an initial guess [10].

A. Continuation of the families of invariant tori

Once an invariant curve has been found, it is possible to continue the solution and obtain a family of invariant tori. Unlike for the families of periodic orbits, which are one-parameter families, invariant tori belong to two-parameter families [10]. Therefore, for consistency, it is necessary to fix one parameter within the family during the continuation. Common choices include the rotation number and the Jacobi constant [10]. In this Note we compute the families of invariant tori at fixed Jacobi constants. Note that if $\psi(\boldsymbol{\theta})$ is an invariant torus, $\psi(\boldsymbol{\theta} + \boldsymbol{\theta}_0)$, with $\boldsymbol{\theta}_0 \in \mathbb{R}^2$ would also be a solution of the problem but not a different torus, i.e., the invariant curve would simply be phased in any of the two angles of the torus. Therefore, in order to compute invariant curves of different tori, two phase constraints are included. Additionally, the pseudo-arclength constraint is used to ensure the next solution is at a certain distance from the previous one, making the distance between solutions the continuation parameter. For the pseudo-arclength constraint, the tangent direction is obtained simply as the normalized difference between two already known solutions. For more details on these constraints, the reader can consult Ref. [10].

V. Results

This section contains the families of quasi-periodic orbits considered in this Note. Families are computed for a lightness number of $\beta = 0.02$ around SL_1, SL_2 and SL_5. Subsequently, the effect of the lightness number is considered.

A. Families of invariant tori around SL_1

We start by studying quasi-periodic motion in the neighborhood of the SL_1 point. Figure 3 showed that for all lightness numbers considered, the planar Lyapunov orbits around the SL_1 point have a central part at the start of the families. When increasing the Jacobi constant value, a pitchfork bifurcation occurs, where the orbits stop being elliptic, giving rise to the halo families [9]. Since invariant tori only exist around periodic orbits that have a central part, the planar Lyapunov orbits have quasi-periodic motion around them before they bifurcate into the halo family and later on when they regain their central part. Nevertheless, invariant tori still exist around both the vertical Lyapunov and halo orbits when $s_i = 2$, see Fig. 5 and Fig. 7. In order to obtain the general picture, we compute the families around planar and vertical Lyapunov orbits as well as around halo orbits for $\beta = 0.02$ for Jacobi values close to the bifurcation of the planar Lyapunov family into the halo family. For visualization, the intersection of the families of quasi-periodic orbits with the ecliptic plane is plotted in Fig. 11. Note that the intersections of the planar and vertical Lyapunov orbits as well as the halo orbits with the ecliptic plane at the Jacobi constant under consideration are represented in black and using black markers. The results, albeit conceptually very different, highly resemble those obtained with the reduction to the center manifold method [8, 9]. Note that, as outlined in the Introduction, the invariant curves obtained can be used to directly parameterize quasi-periodic orbits—instead, the reduction to the center manifold obtains points in quasi-periodic orbits at Poincaré sections in center manifold coordinates.

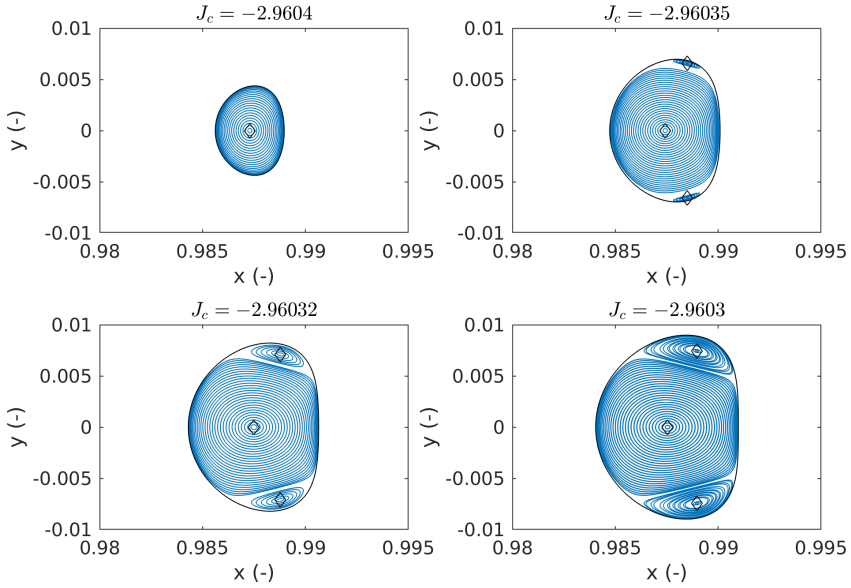

Fig. 11 Intersections with the ecliptic plane of Lissajous and quasi-halo families around SL_1 for $\beta = 0.02$ at different Jacobi constant values.

The figure shows that the quasi-periodic motion is bounded by the planar Lyapunov orbit. The quasi-periodic orbits around the planar and vertical Lyapunov orbits are referred to as Lissajous orbits, whereas those around the halo orbits are referred to as quasi-halo orbits. For Jacobi constant values before the pitchfork bifurcation (see Fig. 11 for

$J_c = -2.9604$), the families of tori around the planar and vertical Lyapunov orbits are connected and all quasi-periodic motion within the planar Lyapunov orbit presents the same structure. Note that by "connected" we mean that both families are the same. It is therefore possible to continue from a planar to a vertical Lyapunov orbit through a family of quasi-periodic orbits. Such a connection was already shown for the CR3BP [2] and the results in Fig. 11 proves that it persists when a solar-sail acceleration is included in the dynamics. Figure 12 shows this connection and demonstrates how the quasi-periodic orbits originate around a vertical Lyapunov orbit and morph into a planar Lyapunov orbit. When the Jacobi constant is increased, (see Fig. 11 for $J_c = -2.96035$) the planar Lyapunov orbits are no longer elliptic and quasi-periodic motion ceases to exist around them until the orbits regain their central part (not shown in Fig. 11). Furthermore, families of quasi-halo orbits start to emerge that increase in size with increasing Jacobi constant.

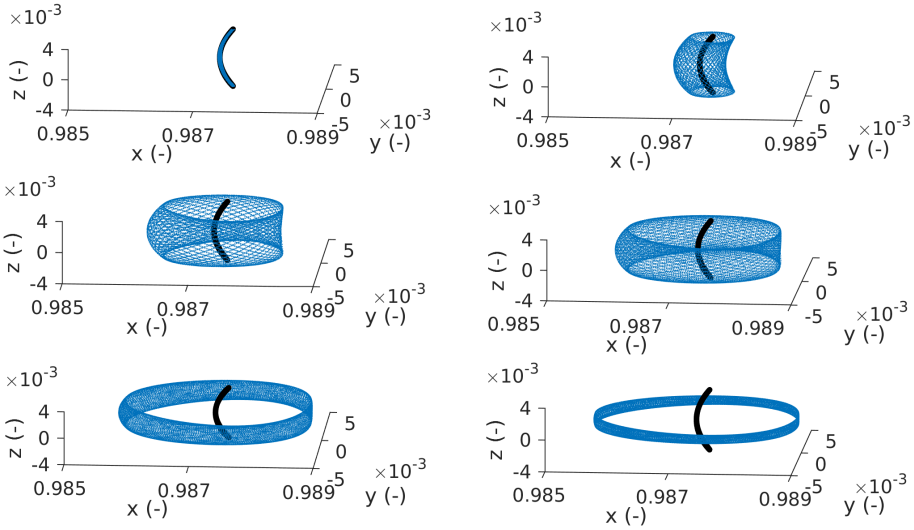

Fig. 12 Evolution of the Lissajous quasi-periodic orbits around a vertical Lyapunov orbit around SL_1 for $\beta = 0.02$ and $J_c = -2.9604$.

It was shown that for the planar Lyapunov families around the SL_1 point, the orbits regain their central part and families of invariant tori again start to exist around them. These orbits are no longer connected to the quasi-periodic orbits that exist around the vertical Lyapunov orbits that were shown in Fig. 12. As an example of such a case, Fig. 13 depicts around the SL_1 point, for $\beta = 0.02$ and $J_c = -2.96$ (see Fig. 3a for $j_c = -0.9985$), quasi-periodic motion around planar and vertical Lyapunov and halo orbits. Similar results can be obtained around the SL_2 point.

B. Families of invariant tori around SL_2

The general picture for quasi-periodic motion around the SL_2 point is very similar to that around the SL_1 point. As was shown in Fig. 3, the stability indices for the planar Lyapunov families around the SL_2 point indicate that the orbits at the start of the families have a central part. When the Jacobi constant is increased, a bifurcation takes place where the orbits become hyperbolic and they lose their central part. This bifurcation gives rise to the families of halo orbits

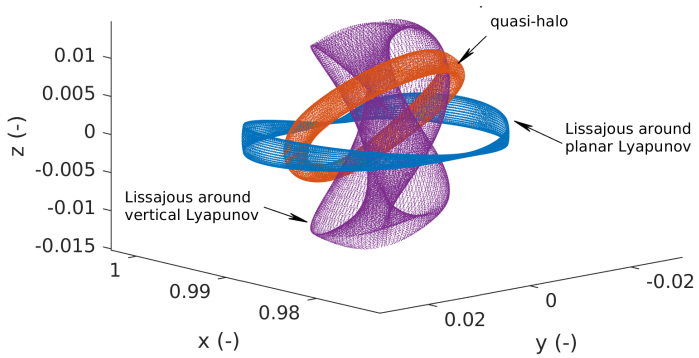

Fig. 13 Examples of quasi-periodic orbits around a planar Lyapunov, a vertical Lyapunov, and a halo orbit around SL_1 for $\beta = 0.02$ and $J_c = -2.96$.

around the SL_2 point. When further increasing the Jacobi constant, the planar Lyapunov orbits regain their central part when $s_2 = 2$. Regarding invariant tori around vertical Lyapunov orbits, Fig. 3 shows that orbits at a wide range of Jacobi constant values have a central part. Therefore, families of Lissajous orbits exist around such orbits. Lastly, for all lightness numbers considered, the halo orbits around the SL_2 point have quasi-periodic motion around them, since, as Fig. 7 shows, $s_2 = 2$ for all orbits. Figure 14 depicts the intersection between the families of tori around the SL_2 point and the ecliptic plane for $\beta = 0.02$. Similar to the quasi-periodic motion around the SL_1 point, the families of invariant tori around vertical and planar Lyapunov orbits are connected when the Jacobi constant is smaller than the value at the bifurcation into the halo family (see Fig. 14 for $J_c = -2.9612$). This connection is further demonstrated in Fig. 15, where it can be seen that the family is very similar to the Lissajous family around SL_1 shown in Fig. 12. The planar Lyapunov family again bifurcates into the halo family and the planar orbits lose their central part, breaking the connection with the Lissajous orbits around the vertical Lyapunov orbits whereas quasi-halo orbits emerge (see Fig. 14 for $J_c = -2.96118$). The quasi-halo families then grow in size with increasing values of J_c.

C. Families of invariant tori around SL_5

The linearized dynamics around the planar and vertical Lyapunov orbits around the SL_5 point are of type center×center; therefore, it is possible to initiate the computation of invariant tori from such orbits with *two* initial guesses given by the two eigenvectors associated with the two eigenvalues within the unit circle. While the two initial guesses for invariant curves around the planar family result in two different families of quasi-periodic orbits, the initial guesses for the quasi-periodic motion around the vertical orbits result in the same family. As an example, we computed the families of quasi-periodic orbits around a planar and a vertical Lyapunov orbit around the SL_5 point for $\beta = 0.02$ and Jacobi constant $J_c = -2.958$ and plotted one member of each family in Fig. 16. The figure shows how, for the quasi-periodic motion around planar Lyapunov orbits in the L_5 region, one of the families corresponds to in-plane

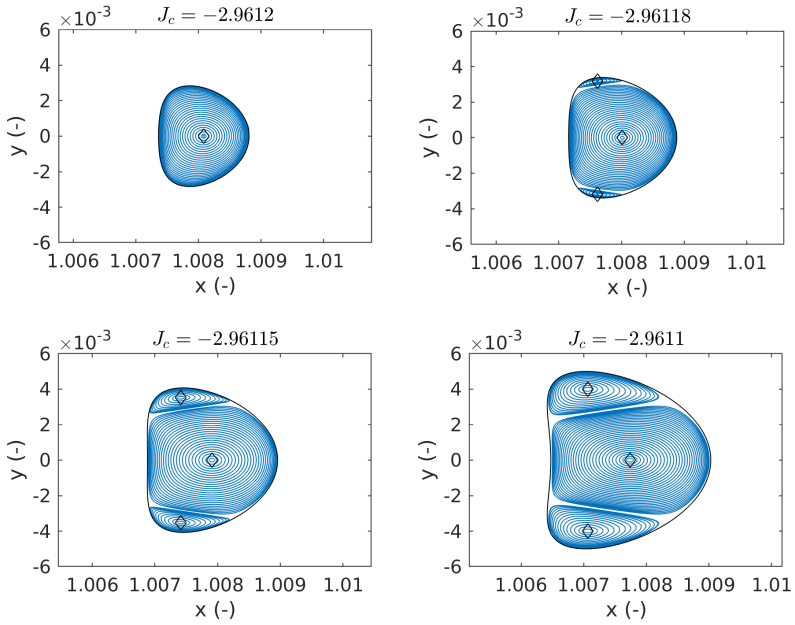

Fig. 14 Intersections with the ecliptic plane of Lissajous and quasi-halo families around SL_2 for $\beta = 0.02$ at different Jacobi constant values.

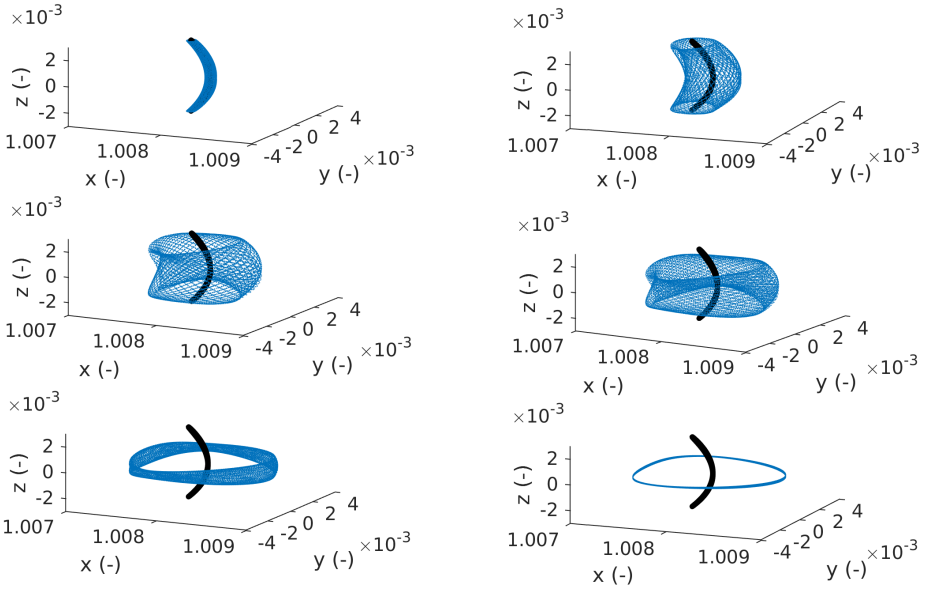

Fig. 15 Evolution of the Lissajous quasi-periodic orbits around a vertical Lyapunov orbit around SL_2 for $\beta = 0.02$ and $J_c = -2.9612$.

quasi-periodic orbits (Fig. 16a) and the second family corresponds to out-of-plane quasi-periodic orbits (Fig. 16b).

D. Evolution of the families of invariant tori with the lightness number

So far, the families of quasi-periodic orbits have been studied for a lightness number of $\beta = 0.02$. This section therefore investigates the effect of the lightness number on the families of quasi-periodic orbits. For such investigation

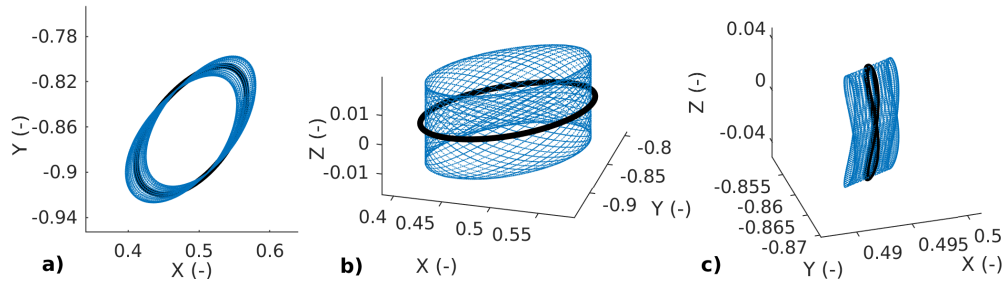

Fig. 16 Quasi-periodic orbits around SL_5 for $\beta = 0.02$ and $J_c = -2.958$: a) In-plane and b) out-of-plane around a planar Lyapunov orbit and c) around a vertical Lyapunov orbit.

we focus on the families of quasi-periodic orbits around the SL_1 point for $\beta \in \{0, 0.01, ..., 0.05\}$.

As it happens for the families of periodic orbits, see Ref. [19]for the halo family, families of quasi-periodic orbits experience some change with the lightness number. In order to compare the families, we compute the intersections between the families of Lissajous and quasi-halo orbits with the ecliptic plane for the lightness numbers considered at comparable values of the Jacobi constant. For each lightness number, we obtain the Jacobi constant value J_c^{bif} where the planar Lyapunov family bifurcates into the halo family and compute the sections at the values $J_c = J_c^{bif} + \Delta J_c$, with $\Delta J_c \in \{-1 \cdot 10^{-5}, 1 \cdot 10^{-5}, 2 \cdot 10^{-5}, 3 \cdot 10^{-5}\}$. Figure 17 depicts the results where the planar Lyapunov orbits are represented with dashed lines and the vertical Lyapunov and halo orbits with black diamonds. Similar to the families for $\beta = 0.02$, see Fig. 11, the planar Lyapunov orbits bound the quasi-periodic motion for all other lightness numbers. Furthermore, the connection of the Lissajous families around planar and vertical Lyapunov orbits persists, see Fig. 17 for $\Delta J_c = -1 \cdot 10^{-5}$. Again, for all lightness numbers considered, increasing the Jacobi constant gives rise to families of quasi-halo orbits, which keep growing in size with increasing ΔJ_c. When the quasi-halo orbits exist, the planar Lyapunov orbits loose their central part and the connection between the families of Lissajous orbits around the planar and vertical Lyapunov orbits is lost. The most noticeable difference is that the families move towards the Sun with increasing lightness number and grow in size. Besides these differences, the families for the lightness number values considered are qualitatively very similar.

E. Applications of solar-sail quasi-periodic orbits

By demonstrating the existence of solar-sail quasi-periodic orbits, the mission design space is significantly increased. Compared to classical QPOs around the L_1 point, these orbits are positioned ever closer to the Sun for increasing lightness number (see Fig. 17). Positioning a solar observatory closer to the Sun than the L_1 point can be leveraged for increasing the warning times for solar storms [12]. The larger sizes of the orbits for increasing lightness number, in particular the size in the out-of-plane direction, may prove beneficial for observing the high-latitudes of the Earth. When comparing the solar-sail QPOs with purely periodic solar-sail orbits, benefits may again be found in the increased design space, in particular in the flexibility in the launch and arrival conditions and satisfying mission requirements and

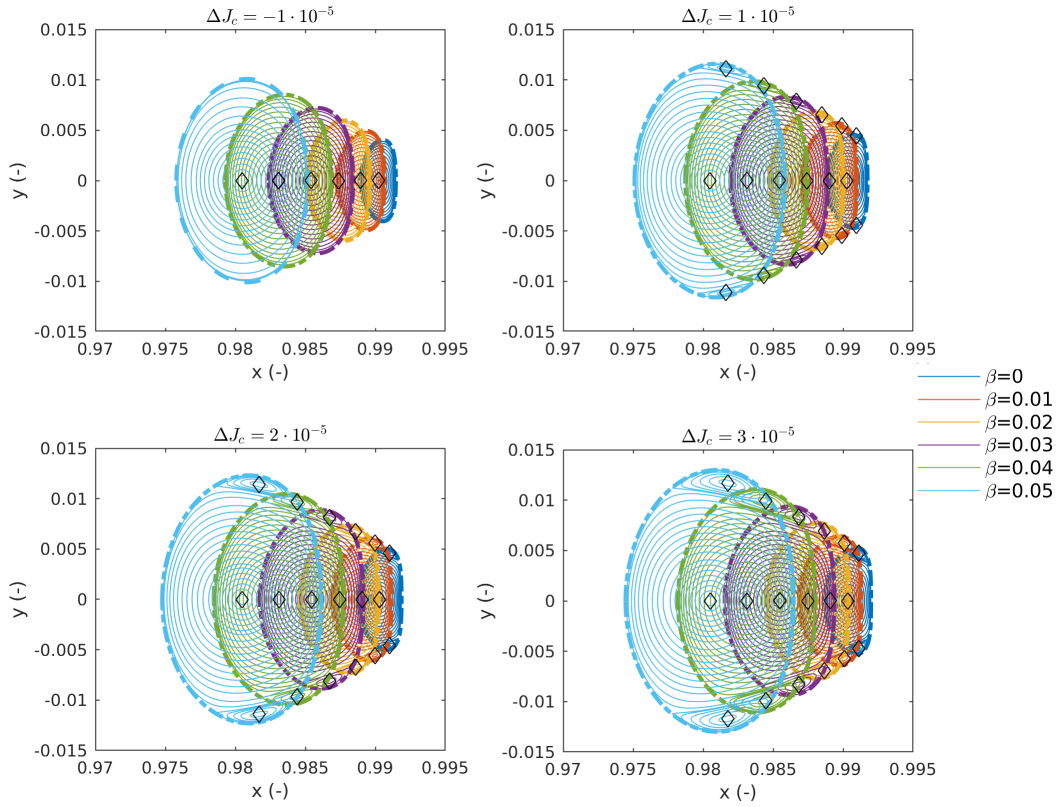

Fig. 17 Intersections between Lissajous and quasi-halo families around SL_1 with the ecliptic plane at different values of ΔJ_c and for different lightness numbers.

constraints. Additional benefits may arise from the increased stability of QPOs over periodic orbits, thereby reducing station-keeping requirements and easing mission operations. Finally, and beyond the scope of mission design, solar-sail QPOs may contribute to a deeper understanding of the celestial motion of natural objects with large area-to-mass ratios, e.g., dust particles, and may therefore aid our understanding of the formation and evolution of our solar system.

VI. Conclusions

This Note investigated solar-sail periodic and quasi-periodic orbits around the displaced first, second and fifth Lagrange points, denoted by SL_1, SL_2 and SL_5, respectively. For the periodic orbits, it was found that, as it happens for the halo family around SL_1, the vertical Lyapunov family around SL_2 also bifurcates into planar orbits for a lightness number, β, close to 0.05. By deriving an extension of the method of invariant curves under stroboscopic maps from the classical to the solar-sail case, solar-sail quasi-periodic orbits were demonstrated to exist around elliptic planar and vertical Lyapunov orbits as well as around elliptic halo orbits for $\beta \in \{0.01, 0.02, 0.03, 0.04, 0.05\}$. Solar-sail quasi-periodic motion around the SL_1 and SL_2 points is bounded by planar Lyapunov orbits as in the classical problem, i.e., without a solar sail. Furthermore, for Jacobi constant values smaller than at the bifurcation of the planar Lyapunov family into the halo family, the families of quasi-periodic orbits around planar and vertical Lyapunov orbits are connected,

while halo or quasi-halo orbits do not exist. For larger values of the Jacobi constant, and as long as the planar Lyapunov orbits do not have a central part, families of quasi-periodic orbits exist around vertical and halo orbits. When the planar orbits regain their central part, different families of quasi-periodic orbits exist around planar and vertical Lyapunov orbits as well as around halo orbits. Regarding the existence of families of solar-sail quasi-periodic orbits around the SL_5 point, the planar and vertical Lyapunov orbits always have a central part and therefore they are always surrounded by quasi-periodic motion. One type of solar-sail quasi-periodic orbit was found around the vertical orbits while two different types of families were found around the planar orbits: in-plane and out-of-plane. Lastly, the study on the evolution of families of quasi-periodic orbits around SL_1 with the lightness number showed that the families are qualitatively very similar. However, with increasing lightness number, the families are displaced towards the Sun and increase in size. Through the use of the method of invariant curves under stroboscopic maps, the quasi-periodic orbits obtained in this Note can be directly used in space mission design analyses as they can be explicitly set as departure or arrival invariant objects.

References

[1] Doedel E. J. et al, "Elemental Periodic Orbits Associated with the Libration Points in the Circular Restricted 3-Body Problem," *International Journal of Bifurcation and Chaos*, Vol. 17, No. 08, 2007, pp. 2625–2677. doi:https://doi.org/10.1142/s0218127407018671.

[2] Gómez, G., and Mondelo, J., "The Dynamics Around the Collinear Equilibrium Points of the RTBP," *Physica D: Nonlinear Phenomena*, Vol. 157, No. 4, 2001, pp. 283–321. doi:https://doi.org/10.1016/s0167-2789(01)00312-8.

[3] Fernandez Mora, A., "Solar-Sail Invariant Objects in the Sun-Earth System and Transfers to the L_5 Region," *Master thesis, Delft University of Technology*, 2019.

[4] Jorba, A., "A Methodology for the Numerical Computation of Normal Forms, Centre Manifolds and First Integrals of Hamiltonian Systems," *Experimental Mathematics*, Vol. 8, No. 2, 1999, pp. 155–195. doi:https://doi.org/10.1080/10586458.1999.10504397.

[5] Kolemen, E., Kasdin, N. J., and Gurfil, P., "Multiple Poincaré Sections Method for Finding the Quasiperiodic Orbits of the Restricted Three Body Problem," *Celestial Mechanics and Dynamical Astronomy*, Vol. 112, No. 1, 2011, pp. 47–74. doi:https://doi.org/10.1007/s10569-011-9383-x.

[6] Baresi, N., Olikara, Z. P., and Scheeres, D. J., "Fully Numerical Methods for Continuing Families of Quasi-Periodic Invariant Tori in Astrodynamics," *The Journal of the Astronautical Sciences*, Vol. 65, No. 2, 2018, pp. 157–182. doi:https://doi.org/10.1007/s40295-017-0124-6.

[7] McInnes, C. R., *Solar Sailing - Technology, Dynamics and Mission Applications*, Springer, 2017, Chaps. 1, 2, 5. doi:https://doi.org/10.1007/978-1-4471-3992-8.

[8] Farrés, A., "Contribution to the Dynamics of a Solar Sail in the Earth-Sun System," *Doctorial thesis, Universitat de Barcelona*, 2009.

[9] Farrés, A., and Jorba, À., "Periodic and Quasi-Periodic Motions of a Solar Sail Close to SL_1 in the Earth-Sun System," *Celestial Mechanics and Dynamical Astronomy*, Vol. 107, No. 1-2, 2010, pp. 233–253. doi:https://doi.org/10.1007/s10569-010-9268-4.

[10] Olikara, Z. P and Scheeres, D. J., "Numerical Method for Computing Quasi-Periodic Orbits and Their Stability in the Restricted Three-Body Problem," *Advances in the Astronautical Sciences*, Vol. 145, 2012, pp. 911–930.

[11] Heiligers, J., Fernandez, J. M., Stohlman, O. R., and Wilkie, W. K., "Trajectory Design for a Solar-Sail Mission to Asteroid 2016 HO3," *Astrodynamics*, Vol. 3, No. 3, 2019, pp. 231–246. doi:https://doi.org/10.1007/s42064-019-0061-1.

[12] Heiligers, J., Diedrich, B., Derbes, W., and McInnes, C., "Sunjammer: Preliminary End-to-End Mission Design," *AIAA/AAS Astrodynamics Specialist Conference*, American Institute of Aeronautics and Astronautics, 2014. doi:https://doi.org/10.2514/6.2014-4127.

[13] Farrés, A., "Transfer Orbits to L_4 with a Solar Sail in the Earth-Sun System," *Acta Astronautica*, Vol. 137, 2017, pp. 78–90. doi:https://doi.org/10.1016/j.actaastro.2017.04.010.

[14] Breakwell, J. V., and Brown, J. V., "The 'Halo' Family of 3-Dimensional Periodic Orbits in the Earth-Moon Restricted 3-Body Problem," *Celestial Mechanics*, Vol. 20, No. 4, 1979, pp. 389–404. doi:https://doi.org/10.1007/bf01230405.

[15] Richardson, D. L., "Halo orbit formulation for the ISEE-3 mission," *Journal of Guidance and Control*, Vol. 3, No. 6, 1980, pp. 543–548. doi:https://doi.org/10.2514/3.56033.

[16] Heiligers, J., Macdonald, M., and Parker, J. S., "Extension of Earth-Moon Libration Point Orbits with Solar Sail Propulsion," *Astrophysics and Space Science*, Vol. 361, No. 7, 2016. doi:https://doi.org/10.1007/s10509-016-2783-3.

[17] Waters, T. J., and McInnes, C. R., "Periodic Orbits Above the Ecliptic in the Solar-Sail Restricted Three-Body Problem," *Journal of Guidance, Control, and Dynamics*, Vol. 30, No. 3, 2007, pp. 687–693. doi:https://doi.org/10.2514/1.26232.

[18] Szebehely, V., *Theory of Orbits: The Restricted Problem of Three Bodies*, Elsevier, 2012, Chap. 8. doi:https://doi.org/10.1115/1.3601280.

[19] Verrier, P., Waters, T., and Sieber, J., "Evolution of the $\mathcal{L}_1$ Halo Family in the Radial Solar Sail Circular Restricted Three-Body Problem," *Celestial Mechanics and Dynamical Astronomy*, Vol. 120, No. 4, 2014, pp. 373–400. doi:https://doi.org/10.1007/s10569-014-9575-2.

[20] Arnold, V. I., *Mathematical Methods of Classical Mechanics*, Springer New York, 1978, Chap. 10. doi:https://doi.org/10.1007/978-1-4757-1693-1.